Glassy ferromagnetism and magnetic phase separation in $La_{1-x}Sr_xCoO_3$

J. Wu and C. Leighton
Department of Chemical Engineering and Materials Science, University of Minnesota, Minneapolis, Minnesota 55455
(Received 18 November 2002; revised manuscript received 27 January 2003; published 14 May 2003)

We present the results of a comprehensive investigation of the dc magnetization, ac susceptibility, and magnetotransport properties of the glassy ferromagnet $La_{1-x}Sr_xCoO_3$. The compositions studied span the range from the end-member $LaCoO_3$ ($x=0.0$) through to $x=0.7$. These materials have attracted attention recently, primarily due to the spin-state transition phenomena in $LaCoO_3$ and the unusual nature of the magnetic ground state for finite x. In this paper we present a consistent picture of the magnetic behavior of $La_{1-x}Sr_xCoO_3$ in terms of short-range ferromagnetic ordering and intrinsic phase separation. At high Sr doping ($x>0.2$) the system exhibits unconventional ferromagnetism (with a Curie temperature up to 250 K), which is interpreted in terms of the coalescence of short-range-ordered ferromagnetic clusters. Brillouin function fits to the temperature dependence of the magnetization as well as high-temperature Curie-Weiss behavior suggest that the Co^{3+} and Co^{4+} ions are both in the intermediate spin state. At lower Sr doping ($x<0.18$) the system enters a mixed phase that displays the characteristics of both a spin glass *and* a ferromagnet. A cusp in the zero-field-cooled dc magnetization, a frequency-dependent peak in the ac susceptibility and time-dependent effects in both dc and ac magnetic properties all point towards glassy behavior. On the other hand, field cooling results in a relatively large ferromagneticlike moment, with zero-field-cooled and field-cooled magnetizations bifurcating at an irreversibility point. Even in the region above $x=0.2$ the out-of-phase component of the ac susceptibility shows frequency-dependent peaks below the Curie temperature (indicative of glassy behavior) which have previously been interpreted in terms of the freezing of clusters. All of the results are consistent with the existence of a strong tendency towards magnetic phase separation in this material, a conclusion which is further reinforced by consideration of the electronic properties. The metal-insulator transition is observed to be coincident with the onset of ferromagnetic ordering ($x=0.18$) and has a behavior in the doping dependence of the low-temperature conductivity which is strongly suggestive of percolation. This can be interpreted as a percolation transition within the simple ferromagnetic cluster model. On the metallic side of the transition the system exhibits colossal magnetoresistance-type behavior with a peak in the negative magnetoresistance ($\sim$10% in 90 kOe) in the vicinity of the Curie temperature. As the transition is approached from the metallic side we observe the onset of a negative magnetoresistance that increases in magnitude with decreasing temperature, reaching values as large as 90% in a 90-kOe field. This magnetoresistance is enhanced at the metal-insulator transition, where it persists even to room temperature.

DOI: 10.1103/PhysRevB.67.174408 PACS number(s): 75.50.Lk, 71.30.+h, 72.15.Gd

I. INTRODUCTION

Magnetic oxides with perovskite (or similar) crystal structures have proven to be a fertile research area for physicists, solid-state chemists, and materials scientists, due to the fascinating array of superconducting, magnetic, and electronic properties they exhibit. These properties range from high-temperature superconductivity,[1] colossal magnetoresistance (CMR),[2,3] and ferroelectricity[4,5] (even simultaneous ferromagnetic and ferroelectric ordering[6,7]) to co-incident metal-insulator, structural, and magnetic phase transitions. In the perovskite manganites alone, materials such as $La_{1-x}Sr_xMnO_3$, $Nd_{1-x}Sr_xMnO_3$, and $Pr_{1-x}Ca_xMnO_3$ exhibit rich phase diagrams involving charge, orbital, canted antiferromagnetic, simple antiferromagnetic, and ferromagnetic orderings.[2] In addition to this richness in magnetic behavior metal-insulator transitions (MIT's) often occur and can even be coincident with structural or magnetic changes due to the strong coupling between charge, magnetic, and lattice degrees of freedom.

Despite their discovery in the 1950s[8,9] (at the same time as the manganites) the perovskite cobaltites have received relatively little attention. This is particularly surprising given the renewed interest in the manganites, which was stimulated to a large extent by the re-discovery of CMR effects in epitaxial thin films and single crystals.[10,11] The cobaltites have received *some* attention however, due to a couple of unique properties; namely, the existence of spin-state transitions[12–16] (and the possibility of rarely observed Co spin states[17–19]) as well as the unusual magnetic ground state of doped cobaltites.[20–24] The former effects are due to the fact that the crystal-field splitting of the Co d states (E_{CF}) and the Hund's rule exchange energy (E_{EX}) are comparable for the cobaltites, meaning that the energy gap between the t_{2g} and e_g states is rather small. In fact, this gap can be of the order of 10 meV in $LaCoO_3$, meaning that t_{2g} electrons can be thermally excited into the e_g states, resulting in higher spin states.[12–16] Spin-state transitions also occur in other cobaltites such as $Pr_{0.5}Ca_{0.5}CoO_3$ (Ref. 25) and $GdBaCo_2O_{5.5}$,[26,27] while the ''intermediate spin state'' (which is seldom observed in Co compounds) has been claimed to exist in $La_{1-x}Sr_xCoO_3$ by several authors.[17–19] The second unusual property of doped cobaltites which has received some attention is the existence of ''glassy ferromagnetism'' in $La_{1-x}Sr_xCoO_3$.[20–24] In essence, the system evolves from a spin-glass or cluster-glass phase at low Sr doping, to a state

that has characteristics associated with ferromagnetic (F) order at higher doping. The boundary between the two, and indeed the exact characteristic of the two phases, is not clear. Higher doping level samples show Brillouin-like temperature dependence of magnetization and an apparent Curie temperature (T_C) but also exhibit signatures of glassy behavior such as frequency-dependent ac susceptibility peaks and time-dependent phenomena. Similarly, the low doping samples exhibit frequency-dependent peaks in the ac susceptibility that can be identified as spin-glass characteristics, but also show large field-cooled magnetizations and an irreversibility temperature, which are suggestive of strong ferromagnetic correlations.

It should be made clear that co-existence of ferromagnetic ordering and glassy behavior is not confined solely to systems like $La_{1-x}Sr_xCoO_3$. In particular, materials such as $Y_{1-x}Ca_xMnO_3$,[28,29] $La_{0.7-x}Y_xCa_{0.3}MnO_3$,[30] $NdBa_2Cu_3O_{7-\delta}$,[31] $Sr_3FeCoO_{7-\delta}$,[32] $La_{0.8}Sr_{0.2}Co_{1-x}Mn_xO_3$,[33] and $La_{0.7}Sr_{0.3}Co_{1-x}Ga_xO_3$ (Ref. 34) all show related behavior. The physics of these mixed phase ferromagnetic/spin-glass systems is also of relevance to re-entrant spin-glass systems (where Au-Fe alloys are the canonical example), particularly perovskites such as $La_{1.2}Sr_{1.8}Mn_2O_7$ (Ref. 35) and $La_{0.46}Sr_{0.54}Mn_{1-y}Cr_yO_3$.[36]

Although this behavior is far from fully understood it is thought to have its origin in the short-range intrinsic magnetic phase separation, which is considered to be a key issue in many other related systems such as cuprates and manganites. In the manganites alone, phase segregation has been observed by various methods such as neutron scattering,[37] scanning tunneling microscopy (STM),[38] temperature-dependent random telegraph noise,[39,40] and time-dependent magnetotransport measurements.[41] From the theoretical point of view many authors have pointed out that these materials are susceptible to magnetic and electronic phase separation even in the absence of chemical phase separation,[42,43] and that this concept can successfully explain many of the features seen in the magnetic and electronic behavior of manganites. Spontaneous magnetic phase separation is thought to be a distinct possibility in situations where a delicate energy balance exists due to close competition between various interactions. Abundant evidence for the existence of competing interactions in materials such as the manganites is provided by the existence of a multitude of ground states, as discussed above.[2] It has also been suggested (on the basis of x-ray-absorption fine-structure data) that materials like $La_{1-x}Sr_xMnO_3$ possess intrinsic chemical and structural inhomogeneity.[44] Such inhomogeneity would be an obvious driving force for magnetic phase segregation. It is worth noting at this point that intrinsic phase separation, in the form of the formation of magnetic polarons, is already viewed as the prime candidate for the explanation of many phenomena exhibited by magnetic and diluted magnetic semiconductors such as EuS,[45] a-Gd_xSi_{1-x},[46] $Gd_{3-x}v_xS_4$ (v=vacancy)[47] and doped $Cd_{1-x}Mn_xTe$.[48] Although the formation and behavior of these entities[49] is far better understood in these classic magnetic semiconductors it seems clear that they share many common features with the perovskite manganites and cobaltites. In cobaltite materials specifically, many of the magnetic properties can be simply explained by the formation of short-range-ordered ferromagnetic clusters. Spin-glass (SG) ordering at low doping is then understood in terms of the frustration between the F order in the clusters with the antiferromagnetic (AF) interactions present in the background matrix. These ferromagnetic clusters eventually coalesce, leading to apparent ferromagnetic ordering.

In this paper we investigate in detail the magnetic and magnetotransport properties of $La_{1-x}Sr_xCoO_3$. We have studied 14 compositions in the range $0.0<x<0.70$, in polycrystalline bulk material. Combining dc magnetization measurements after field cooling (FC) and zero-field cooling (ZFC), ac susceptibility measurements as a function of frequency, ferromagnetic hysteresis loops, and the field and temperature dependence of the resistivity, we are able to build an understanding of the empirical behavior in the whole of the interesting composition range. We are able to systematically ''track'' the evolution from the short-range-ordered FM state to the SG-like state at low doping. In the ferromagnetic phase we still observe frequency-dependent phenomena in the out-of-phase component of the ac susceptibility (suggesting that some glassy behavior still persists), as well as metallic behavior and CMR-type magnetoresistance. Both Co ions (Co^{3+} and Co^{4+}) are determined to be in the ''intermediate spin state'' from the temperature dependence of the spontaneous magnetization in the ferromagnetic state and from the Curie-Weiss behavior in the paramagnetic state. As the Sr content is lowered the F dominant state is lost and the SG characteristics dominate, although large FC magnetizations still exist, as well as a noteworthy irreversibility line. The CMR is decreased with decreasing Sr doping level, and an additional low-temperature negative MR component is observed. Eventually a MIT occurs (at $x \approx 0.18$), coincident with the loss of FM order. We interpret our data in terms of the short-range order ''cluster model'' which qualitatively explains this behavior. Finally, we suggest that these materials exhibit a tendency towards phase separation which is even stronger than that seen in the manganites suggesting that doped cobaltites could be model systems for the investigation (both theoretical and experimental) of magnetic phase separation.

II. EXPERIMENTAL CONSIDERATIONS

Polycrystals of $La_{1-x}Sr_xCoO_3$ ($0.0<x<0.70$) were fabricated from La_2O_3, Co_3O_4, and $SrCO_3$ starting materials by the standard solid-state reaction method. The starting powders were thoroughly ground, calcined in air for 7 days at 980 °C, then furnace cooled over a period of 6 h to room temperature. The reacted powders were then cold pressed under 8000 psi into disks of thickness ~1 mm. These disks were sintered in air for 1 day at 1200 °C and then slow cooled over a period of 24 h. Structural characterization was performed by high-resolution x-ray diffraction (XRD), scanning electron microscopy (SEM), energy dispersive analysis of x rays (EDAX) and iodometric titration. In particular XRD was performed at regular intervals to monitor the progress of the reaction. A typical XRD diffraction pattern is shown in Fig. 1 (for $x=0.30$), confirming that, at least within

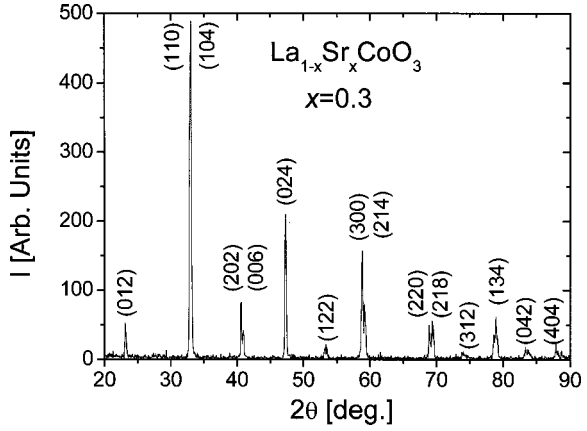

FIG. 1. Wide angle powder x-ray-diffraction spectrum of an $x=0.30$ sample taken with Cu K_α radiation.

the sensitivity of XRD, the samples are single phase and have the expected lattice parameter ($a=5.42$ Å and $c=13.26$ Å, for $x=0.30$). It is worth noting that we do not observe any magnetic anomalies at any of the expected transition temperatures of other cobalt oxides (Co_3O_4, CoO, etc.) or any other foreign phases, further evidence that the samples are single phase. The crystal structure is rhombohedral for $x=0$ and shows a reduction in the rhombohedral distortion with increasing x. In fact for $x>0.5$ the structure is cubic. The broadening of the reflections, which can be quantified via the full width at half maximum of the various peaks, is due to the effects of grain size and microstrain. The relative importance of the two contributions can be deconvoluted with a Williamson-Hall analysis that allows us to investigate the microstrain and its dependence on Sr doping. This is depicted in Fig. 2, which shows the effect of Sr doping on the microstrain before and after the final sintering step. It is clear that the considerable strain that is introduced into the lattice by Sr doping is relieved by sintering at 1200 °C for 1 day. SEM revealed that the average grain size

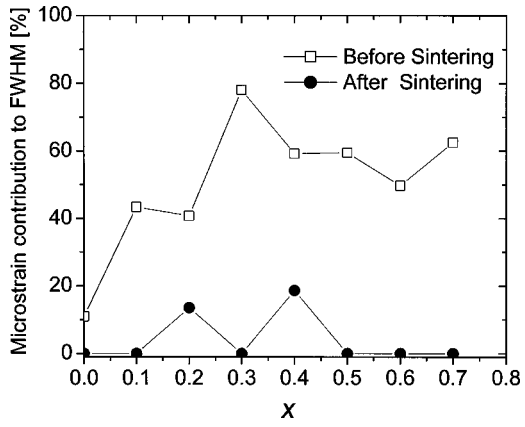

FIG. 2. The doping dependence of the microstrain contribution to the full width at half maximum of the XRD peaks before (open symbols) and after (closed symbols) the final 1200 °C sintering step. The peak broadening is due to microstrain and grain size effects. These were deconvoluted using a Williamson-Hall analysis of the $n(110)$ reflections.

of our material is of the order of 10 μm, independent of Sr doping level. EDAX was used to check the overall stoichiometry of the samples, as well as to probe the compositional fluctuations. Within experimental uncertainty we determined that the composition within a grain is identical to that seen at grain boundaries, and that the composition of multiple grains are identical. Measuring the La/Sr ratio every 2 μm along a 20-μm-long, randomly chosen straight line results in a standard deviation of 4.8% for an $x=0.5$ sample, which should be compared to an experimental uncertainty of 6.1%. Finally, a small number of samples had their oxygen content probed by iodometric titration resulting in a measured oxygen stoichiometry of $La_{1-x}Sr_xCoO_{2.98\pm0.03}$. In summary, the samples are single phase, large grain size, stoichiometric polycrystals with small compositional fluctuations.

The magnetic measurements were made in a commercial superconducting quantum interference device (SQUID) magnetometer and a commercial dc extraction magnetometer in the temperature range $4<T<300$ K and in magnetic fields up to 50 kOe. ac susceptibility measurements were also made in a commercial system in the frequency range 10 Hz $<f=\omega/2\pi<10$ kHz and over the same temperature interval as dc measurements. An ac driving field of 10 Oe was employed and ''zero-field'' cooling was performed in fields of less than 0.1 Oe. For higher temperature measurements of the dc susceptibility vs temperature a commercial vibrating-sample magnetometer (VSM) was used. Finally, magnetotransport measurements employed an ac excitation at 13.7 Hz and were made in the interval $4.5<T<300$ K in fields up to 90 kOe. The magnetic field was aligned perpendicular to the sample plane, and therefore the current direction. A small number of samples in the vicinity of the metal-insulator transition were measured down to 0.4 K in a commercial He^3 refrigerator. Again a 13.7-Hz ac excitation was used and great care was taken to ensure that sample self-heating effects were negligible.

III. RESULTS AND DISCUSSION

dc magnetization, ac susceptibility and magnetotransport measurements are discussed in turn in Secs. III A, III B, and III C, respectively.

A. dc magnetization

1. Basic magnetic properties and the phase diagram

The temperature dependence of the dc magnetization (measured in a static field of 10 Oe) is shown in Fig. 3, for five representative samples ($x=0.50$, 0.20, 0.18, 0.15, and 0.09). It must be stressed that more samples were measured, at a total of 14 compositions, but only five are presented for the purposes of clarity. Both FC and ZFC data are presented, where the field cooling was performed in 10 Oe. The $x=0.50$ and 0.20 data are representative of all compositions in the range $0.2<x<0.7$; FC curves show a ''Brillouin-like'' temperature dependence of the magnetization[50] and a T_C which reaches a maximum value of 250 K at $x=0.5$, at which point the saturation magnetization is approximately 10 000 emu/mol. In contrast, the ZFC magnetization is rather

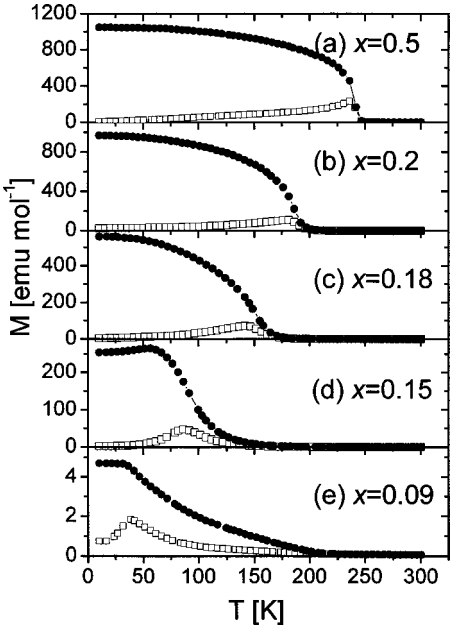

FIG. 3. Temperature dependence of the dc magnetization for $x = 0.50$ (a), 0.20 (b), 0.18 (c), 0.15 (d), and 0.09 (e). ZFC curves are shown as open symbols, whereas FC curves are shown as solid symbols.

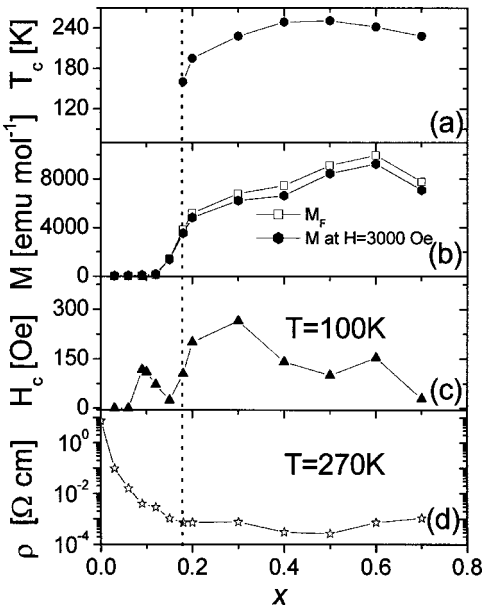

FIG. 4. Sr doping dependence of (a) T_C, (b) M ($H = 3000$ Oe), (c) H_C ($T = 100$ K) and (d) ρ ($T = 270$ K). T_C was estimated from Brillouin fits as described in Sec. III A 2.

low and shows a nonmonotonic behavior with a peak at some temperature T_A which is approximately 5–20 K below T_C, depending on the exact composition. Such data have been observed before in several works[20–24] and are typically interpreted in terms of the ferromagnetic (short-range-ordered) cluster model. It is postulated that the system phase separates into hole-rich ferromagnetic clusters dominated by the ferromagnetic double exchange interaction between Co^{3+} and Co^{4+}, the clusters being embedded in a hole-poor nonferromagnetic matrix.[20–24] This matrix is dominated by the Co^{3+}-Co^{3+} interaction, which is known to be antiferromagnetic (AF) superexchange,[51] as is the Co^{4+}-Co^{4+} interaction. In essence, the concept is that upon zero-field cooling the clusters freeze into random orientations, dictated by a ''local anisotropy field.'' When field cooled the clusters align, leading to the onset of a large ferromagnetic-type magnetization. The existence of a peak in the ZFC magnetization at T_A is then interpreted in terms of a competition between the random local magnetization orientations of the individual clusters and the applied magnetic field. It should be noted that according to this model the hysteresis loops of $La_{1-x}Sr_xCoO_3$ for $x > 0.2$ (the F regime) should not saturate at moderate magnetic fields due to the finite number of Co spins in the nonferromagnetic matrix (where the interactions are of AF type). This is indeed the case, and is discussed later. It is also noteworthy that previous measurements of the field dependence of the temperature at which the ZFC magnetization reaches a maximum show a behavior that is consistent with the de Almeida-Thouless line[52] (a line in the H-T plane), a theory which was originally developed for SG systems. As pointed out by Nam and co-workers[20,21] this is further evidence that the peak in the ZFC magnetization is due to a competition between the random orientation of short-range-ordered clusters and the external field.

As x is decreased to 0.18 the behavior of the FC magnetization is not qualitatively altered but the ZFC magnetization begins to show a sharper cusp at a temperature which is now significantly below T_C. As x is decreased further to 0.15 and eventually 0.09 the FC magnetization no longer shows a simple ''Brillouin-like'' ferromagnetic behavior and is considerably reduced in magnitude. Simultaneously the ZFC magnetization begins to show a sharp cusp at a temperature that decreases with decreasing Sr content down to 0.03. In summary, the ferromagneticlike behavior in the FC magnetization disappears below $x = 0.18$, at which the point the FC magnetization begins to show nontrivial temperature dependence and the ZFC magnetization begins to resemble the characteristic SG cusp. Canonical SG systems typically display a bifurcation of the ZFC and FC magnetizations only very close to T_f, the SG freezing temperature,[53] but in this case the point at which bifurcation occurs (the irreversibility temperature, $T_{\rm irr}$) is $\gg T_f$. In some respects this resembles ''cluster-glass'' behavior as pointed out by several authors (e.g., Ref. 22). A curious aspect of the data for samples with $x < 0.15$ is the unusual doping dependence of $T_{\rm irr}$, a point which will be returned to later in this paper.

The Sr doping dependence of T_C, M, and the 100 K coercivity H_C are shown in Fig. 4, where the existence of a critical Sr doping level for the onset of ferromagnetic ordering (at $x = 0.18$) is clear. T_C, M, and H_C all show a sharp increase around $x = 0.18$ with a maximum in T_C occurring at $x = 0.5$. This maximum in T_C is simply explained by the fact that at $x = 0.50$ the 1:1 ratio of Co^{3+} to Co^{4+} maximizes the strength of the double exchange interaction. This leads to a simultaneous optimization of the electron transfer and a minimum in the resistivity (ρ), as shown in Fig. 4(d). (The electronic transport properties are returned to in more detail

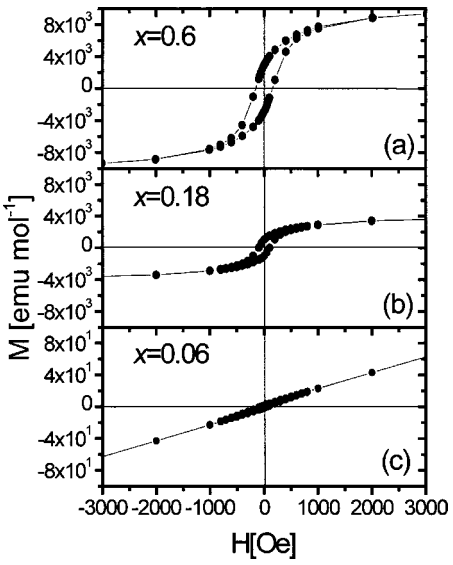

FIG. 5. Hysteresis loops [$M(H)$ curves] for (a) $x=0.60$, (b) $x=0.18$, and (c) $x=0.06$. In all cases the temperature is 100 K. Loops were measured by starting at large positive field, sweeping to negative field, and then returning to positive field.

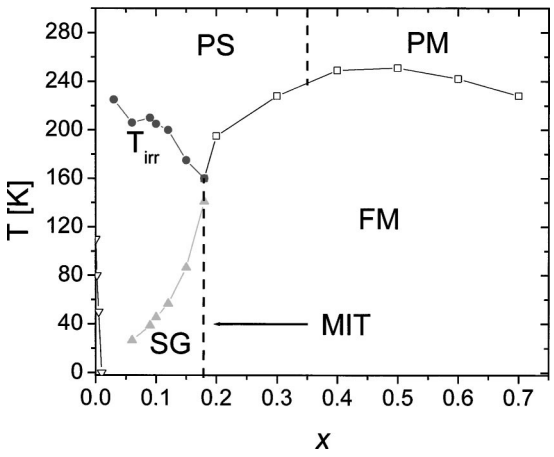

FIG. 6. Magnetic phase diagram (in the *T*-*x* plane) for $La_{1-x}Sr_xCoO_3$. PS=paramagnetic semiconductor, PM=paramagnetic metal, FM=ferromagnetic metal, SG=spin glass, MIT=metal-insulator transition, and T_{irr} is the irreversibility temperature which marks the bifurcation of ZFC and FC dc magnetization curves. The open triangles at very low x indicate the estimated spin-state transition temperature from Yamaguchi *et al.* (Ref. 14).

in Sec. III C.) The magnetization values displayed in Fig. 4 are for an applied field of 3 kOe, rather than simply quoting saturation values. This is done because even in the ferromagnetic phase at $x \gg 0.18$ the magnetization does not saturate in fields up to 50 kOe. Representative hysteresis loops at $T=100$ K are shown in Fig. 5 for $x=0.60$, 0.18, and 0.06. The $x=0.60$ and 0.18 loops are representative of all samples at $x>0.18$, showing ferromagnetic behavior with clear hysteresis, in addition to a component of the magnetization which does not saturate. This is consistent with the simple cluster model where some fraction of the Co spins exist in the nonferromagnetic matrix, where the interactions are AF. A simple method to completely separate the F contribution from the non-F spins in the AF matrix is to recognize that the high-field magnetization is given by $M_F+\chi_{AF}H$, where M_F is the F component and χ_{AF} is the slope of M vs H at high field. Extrapolation of this high-field behavior back to $H=0$ therefore gives the F component only. Hence in Fig. 4(b) we show two M values; data obtained at $H=3$ kOe and the true M_F values. As can be seen from the figure the two methods are in close agreement. As a final comment on the doping dependence of these basic magnetic parameters it is worth pointing out that H_C is temperature dependent, showing a significant increase with reducing T in the F phase. H_C values as large as 600 Oe are obtained at 10 K, which could be related to the inhomogeneous magnetic ground state.

Combining these data we are able to construct a magnetic phase diagram similar to that of Itoh *et al.*[24] as shown in Fig. 6. We have also included the behavior of the $x=0$ compound and the evolution of the $LaCoO_3$ MIT and spin-state transitions with very low Sr doping from Yamaguchi *et al.*[54] The phase diagram is dominated by the transition at $x=x_c$ ($0.15<x_c<0.18$) from the regime where the FC magnetization shows F ordering, to the regime at $x<x_c$ where the magnetism is dominated by the SG-type behavior. The T_C monotonically decreases with decreasing x, from $x=0.5$ down to $x=0.18$, below which the phase diagram is dominated by T_f, which decreases with decreasing x. We propose that the critical point x_c marks the point where the ferromagnetic clusters coalesce allowing for ferromagneticlike temperature dependence of the magnetization when the system is field cooled and the clusters are aligned. The existence of a finite T_C at the point at which the F ordered phase is entered is strong evidence for percolating ferromagnetic clusters. Starting from very low x, the system is originally dominated by AF interactions between Co^{3+} ions. As x is increased and the fraction of Co^{4+} ions increases the system phase separates into ferromagnetically interacting hole-rich clusters in an antiferromagnetically correlated matrix. In the context of our interpretation of the phase diagram in terms of these ferromagnetic clusters it is important to note that they have been studied directly by transmission electron microscopy (TEM) in $La_{1-x}Sr_xCoO_3$, by Caciuffo *et al.*[55] High-resolution images were indicative of an inhomogeneous distribution of La ions leading to hole-rich regions in a hole-poor matrix, with the phase separation occurring on length scales of the order of 10 nm. As the F clusters grow with increasing x the temperature at which the F and AF interactions compete and spin-glass freezing occurs, increases. Hence the $T_f(x)$ line increases monotonically with x, eventually joining with the $T_C(x)$ line at the point (x_c) at which the clusters coalesce. The SG phase is achieved due to the frustration between the AF superexchange (between Co^{3+}-Co^{3+} and Co^{4+}-Co^{4+}) and the ferromagnetic double exchange (Co^{3+}-Co^{4+}). It is in this regime that we observe irreversibility between ZFC and FC magnetization in addition to a relatively large field-cooled magnetization. One simple explanation of this behavior is that the ferromagnetically interacting spins within the clusters respond to the cooling field, leading to the onset of a large FC moment at the

same time as SG behavior, which is due to the competition between F double exchange and AF superexchange. Alternative explanations have been advanced based on cluster glass concepts,[22] as well as superparamagnetic behavior in the F correlated clusters.[56] In the latter work[56] Senaris-Rodriguez *et al.* postulate that the bifurcation of ZFC and FC magnetization curves in this regime is due to the different temperature dependence of ZFC and FC magnetizations of clusters with volumes below the superparamagnetic limit. Looking at Fig. 6 the problem with interpreting our data with either of these models is the anomalous behavior of $T_{\rm irr}$ with Sr doping level. In contrast to Ref. 56 we observe that $T_{\rm irr}$ actually *decreases* with increasing x, meeting with the $T_C(x)$ and $T_f(x)$ lines at the critical point x_c. This would imply that the freezing temperature of the superparamagnetic clusters is decreasing with increasing volume (i.e., increasing x), contrary to our expectations. We are unable to explain the $T_{\rm irr}(x)$ behavior although it is clear that the facts that $T_{\rm irr}$ decreases with x and that the three phase boundaries meet at x_c are critical.

The dissimilarity between the phase diagram of $La_{1-x}Sr_xCoO_3$ shown in Fig. 6 and that of $La_{1-x}Sr_xMnO_3$ (Ref. 2) is striking, and is worthy of some comment. This is primarily due to the fact that the $x=0$ compound $LaCoO_3$ is a diamagnetic semiconductor at $T=0$, unlike $LaMnO_3$ which exhibits AF ordering with $T_N \approx 150$ K. The $La_{1-x}Sr_xMnO_3$ phase diagram shows an AF charge ordered insulating phase at low x which eventually evolves into a ferromagnetic insulator then a ferromagnetic metal.[2] Above $x=0.45$ AF order reappears.[2] In the cobaltite case there has been some suggestion of orbital ordering effects at $100<T<500$ K for $x=0$,[19] but these effects, and the spin-state transitions, are rapidly destroyed with increasing x. Intriguingly, the very low x regime ($x<0.01$) shows magnetic behavior which is suggestive of magnetic polaron formation.[54] These polarons could well be the precursors of the ferromagnetically correlated clusters that dominate the behavior at larger x. Indeed, the distinction between ''magnetic polaron'' and ''short-range-ordered ferromagnetic cluster'' is quite arbitrary in our opinion.

In summary, the $La_{1-x}Sr_xCoO_3$ compound displays a crossover from an SG dominated phase at $x<0.18$ to a F dominated phase at $x>0.18$, although in both cases neither ground state is entirely pure. Following previous works, which were stimulated by the blurred distinction between the SG and F phases in this compound, we undertook an ac susceptibility investigation as discussed in Sec. III B.

2. Determination of the spin state of the Co ions

To shed some light on the spin state of the Co ions we attempted to deduce the Co ion spin value by two simple methods. First we fitted the temperature dependence of the ferromagnetic magnetization to a Brillouin function for each value of x, and extracted the best-fit value of the average Co spin, $S_{\rm avg}(x)$. In the second method we extracted $S_{\rm avg}(x)$ from the Curie-Weiss behavior in the paramagnetic phase at $T>T_C$. Note that another seemingly simple probe of the spin values—measuring the saturation moment in μ_B per Co ion—is fraught with complications due to the lack of saturation in $M(H)$, as previously discussed.

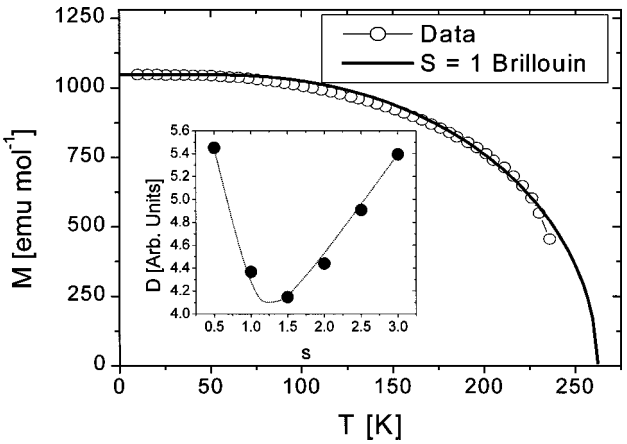

FIG. 7. M vs T for $x=0.5$. The points represent the experimental data while the dotted line is an $S=1$ Brillouin function fit. The data were taken after cooling from 300 to 5 K in a 10-Oe field. The measuring field was 10 Oe. Inset: The deviation (D) between the data and Brillouin function, as a function of the chosen spin value S.

$$D=\sqrt{\frac{\sum_{i=1}^{N}(M_i-M_{\rm Brillouin})^2}{N}}$$

where M_i is the ith data point, $M_{\rm Brillouin}$ is the value of the theoretical Brillouin function, and N is the total number of data points. The dotted line is a guide to the eye.

Figure 7 shows the temperature dependence of the magnetization M (for $x=0.5$) taken in a 10-Oe applied field, after field cooling from 300 to 5 K in a field of 10 Oe. The solid line is the $S=1$ Brillouin function which is a reasonable description of the data. The best fit was determined by finding the S value which minimizes the statistical deviation (D) between the fit and data, as shown in the inset of Fig. 7. (The exact definition of D is provided in the figure caption.) The result of this procedure is a best-fit value of $S=1.25$. Interestingly, repeating our fitting procedure for all other x values results in almost the same spin value, $S\approx 1.25$. This is most clearly illustrated in Fig. 8 which shows the reduced magnetization $[M/M(T=0)]$ vs the reduced temperature (T/T_C) for all six samples in the range $0.2<x<0.7$. The data collapse to a single curve showing that the spin value is independent of x, being approximately 1.25 in all cases. The exact same fitting procedure was also applied to the temperature dependence of the saturation magnetization recorded using larger cooling fields and in larger measuring fields. It was found that the reduced magnetization vs reduced temperature curves always collapse in the range $0.2<x<0.7$, regardless of the exact value of the cooling field and measuring field (fields used were in the range $0<H<100$ Oe). It is important to stress the point that even if the extraction of a definite spin value from the fit shown in Fig. 7 is considered unsatisfactory, the data collapse shown in Fig. 8 proves that the spin values is independent of x (at least for $0.2<x<0.7$), regardless of the confidence in the exact value of S.

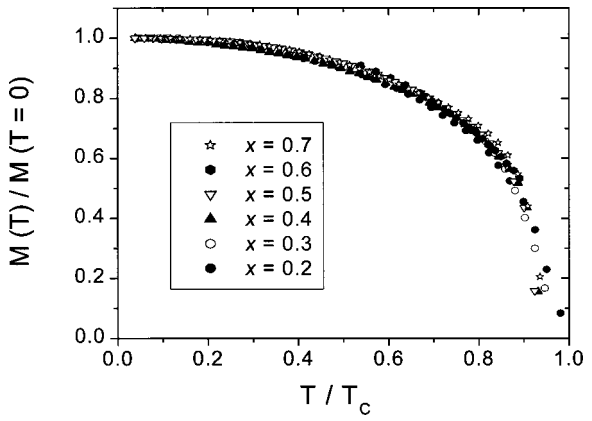

FIG. 8. M (normalized to the $T=0$ value) vs T (normalized to T_C) for six samples in the range $0.2<x<0.7$. As for Fig. 7, the cooling and measuring fields were both set at 10 Oe.

The results from our second method to determine $S_{\text{avg}}(x)$ are displayed in Fig. 9. This method examines the paramagnetic phase where the susceptibility follows the Curie-Weiss law,

$$\chi=\frac{C}{T-\theta}, \tag{1}$$

where

$$C=\frac{N\mu_{\text{eff}}^2}{3k_B} \quad \text{and} \quad \mu_{\text{eff}}=g[J(J+1)]^{1/2}\mu_B. \tag{2}$$

Here, χ is the susceptibility, C is the Curie constant, $\theta \approx T_C$, N is the number of Co ions per m^3, μ_{eff} is the effective number of Bohr magnetons (μ_B), g is the Landé g factor, and J is the total spin quantum number. For all x values Eq. (1) describes the data very well at high temperatures as illustrated in the inset of Fig. 9 for $x=0.5$, which plots χ^{-1} vs T. The slope provides the spin value S_{avg} while the intercept yields θ. (All the θ values extracted in this manner are comparable to T_C.) The values of S_{avg} are then plotted against x in Fig. 9, confirming the conclusion from the previous analysis that the spin values always lie in the range $1<S<1.5$ and are largely independent of Sr doping level. Note that our data reveal no distinct changes in slope in the χ^{-1} vs T curves, suggesting that thermally driven spin-state transitions [such as those observed in the undoped cobaltite $LaCoO_3$,[12–16] $GdBaCo_2O_{5.5}$,[26,27] and $Pr_{0.5}Ca_{0.5}CoO_3$ (Ref. 25)] do not take place in this material (at least in the range $0.2<x<0.7$).

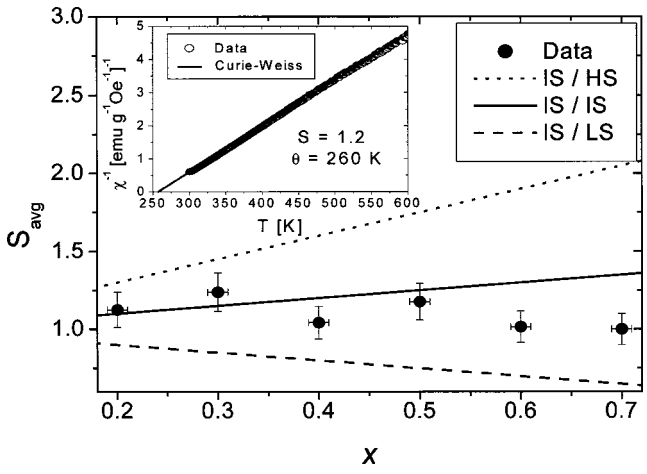

FIG. 9. x dependence of the average spin value (S_{avg}) extracted from the Curie-Weiss behavior at high T. The dotted line assumes IS Co^{3+} and HS Co^{4+}. The broken line assumes IS Co^{3+} and LS Co^{4+}. The solid line assumes IS Co^{3+} and IS Co^{4+}. Inset: χ^{-1} vs $T(T>T_C)$ for $x=0.5$. Solid line is the Curie-Weiss fit.

TABLE I. The possible spin states of the Co^{3+} and Co^{4+} ions in $La_{1-x}Sr_xCoO_3$. The lower energy levels correspond to the t_{2g} electrons, while the highest levels (which are separated from the lower ones by a gap) correspond to the e_g states.

Spin-state	Co^{3+}	Co^{4+}
LS (low spin)	S = 0	S = 1/2
IS (intermediate spin)	S = 1	S = 3/2
HS (high spin)	S = 2	S = 5/2

Denoting the spin of Co^{3+} and Co^{4+} ions as S^{3+} and S^{4+} we can write the average spin value in $La_{1-x}Sr_xCoO_3$ as

$$S_{\text{avg}}=(1-x)S^{3+}+xS^{4+}=S^{3+}+x(S^{4+}-S^{3+}). \tag{3}$$

Clearly the only way to obtain an S_{avg} which is independent of x is to have $S^{3+}=S^{4+}$. The complicating factor in cobaltites is the existence of various spin states, very close in energy, as summarized in Table I. Recent theoretical works clearly favor the intermediate-spin (IS) state for the Co^{3+} ion in $LaCoO_3$,[18,19] but the spin state of the Co ions in $La_{1-x}Sr_xCoO_3$ is more controversial. Although the IS state can be expected for Co^{3+}, due to the suppression of the low-spin (LS) state with very small Sr doping (as shown in the phase diagram, Fig. 6) the spin state of the Co^{4+} ion is an open issue. One should bear in mind that intermediate or high-spin states for Co^{4+} ions are somewhat surprising as in other compounds Co^{4+} favors the low-spin state. The situation where Co^{3+} ions are in the intermediate-spin state ($S^{3+}=1$) and the Co^{4+} ions are in the high-spin state ($S^{4+}=2.5$), as is commonly assumed, is shown as a dotted line in Fig. 9. Clearly our data are at variance with these

assumptions. Moreover, the situation where Co^{3+} ions adopt the IS state and Co^{4+} ions are in the LS state is also a poor description of the data, as shown by the broken line in Fig. 9. In fact, examining Table I it is clear that the only situation which is consistent with the Co^{3+} and Co^{4+} spin values being approximately equal *and* close to 1.25 is the one where both ions are in the intermediate-spin state [i.e., $S=1$ for Co^{3+} ($x=0$) and $S=1.5$ for Co^{4+} ($x=1$)]. This is shown as the solid line in Fig. 5 and is clearly in far better agreement with our data than the assumption of high-spin state or low-spin state Co^{4+}. Note that the data of Fig. 7 and the inset of Fig. 9 (which both deal with the $x=0.5$ case) are perfectly consistent with this hypothesis, as $S=1.25$ is the expected spin value for $x=0.5$.

This situation where both Co ions are in the intermediate-spin state has been recently proposed by Ravindran *et al.*[18] (from spin-density-functional band-structure calculations employing the fixed spin moment method), who suggest that hole doping in this material reduces ionicity, enhancing hybridization between Co and O, and stabilizing the intermediate-spin state. They assert that hole doping in $La_{1-x}Sr_xCoO_3$ uniformly affects all Co ions, meaning that the spin states of the two ions are identical. Due to this Co-O hybridization the expected average Co moment ($1.98\mu_B$/Co for $x=0.5$) is reduced compared to the simple ionic model prediction ($2.5\mu_B$/Co). Although the difficulties with determining the saturation magnetization of these cobaltites have already been noted, our best estimate for $x=0.5$ lies at $1.92\mu_B$/Co, in excellent agreement with the predicted value of $1.98\mu_B$/Co. Our observation of an IS spin state from magnetometry measurements on samples in the range $0.2<x<0.7$ is also consistent with the previous neutron-scattering measurements[17,55] and adds further weight to these arguments. It should be noted that some of these studies deal only with a single composition ($x=0.5$),[17] while our measurements reinforce the point that *the intermediate spin state is stable over a very wide composition range*, and that this can be deduced from very simple magnetometry measurements. It should also be noted that our data are in agreement with the work of Caciuffo *et al.*,[55] who suggest that it is the Co ions in the ferromagnetic clusters that are in the IS state. It is clear that the measurements of ferromagnetic magnetization presented in Fig. 8 probe primarily the Co spins in these ferromagnetic clusters.

We would like to reiterate the point that we observe no evidence of any spin-state transition in the interval $5<T<800$ K, for compositions in the range $0.2<x<0.7$. The existence of both ions in an intermediate-spin state may be consistent with the fact that we observe no evidence for these thermally driven spin-state transitions. As pointed out by Ravindran *et al.*[36] and Korotin *et al.*,[11] the energy gap between the intermediate- and high-spin states is far larger than the gap between the low-spin and intermediate-spin states, meaning that compounds such as $La_{1-x}Sr_xCoO_3$ with an intermediate-spin ground state (at least for $0.2<x<0.7$) are unlikely to display thermal excitation to the high-spin state.

To summarize our attempts to determine the spin state of the Co ions in the F state of $La_{1-x}Sr_xCoO_3$, we have determined the average spin value as a function of x from Brillouin function fits to the behavior below T_C and from Curie-Weiss fits to the behavior above T_C. In both cases this spin values is relatively x independent and is consistent with *both* Co ions adopting the intermediate-spin state.

B. ac susceptibility

The temperature dependence of the ZFC ac susceptibility is displayed in Fig. 10 for 4 representative samples with $x=0.40$, 0.30, 0.18, and 0.09. Both χ' and χ'' (the in-phase and out-of-phase components, respectively) are measured at 10, 100, 1000, and 10 000 Hz. In the F regime at $x>0.18$ all samples display a strong peak in χ', followed by a monotonic decrease as $T\rightarrow 0$. Given the proximity to T_C, and the frequency-independent nature of the peak, this is interpreted as the onset of ferromagnetic ordering. It should be noted that FC $\chi'(T)$ shows similar behavior to ZFC $\chi'(T)$, the only discernible difference being a larger peak value of the susceptibility in the FC case. As expected from the previously discussed behavior of $T_C(x)$, the temperature at which χ' reaches a maximum decreases as x is decreased towards 0.18, where the indication of the onset of ferromagnetic ordering is lost. Below $x=0.18$ all samples show a frequency-dependent peak which occurs very close to the point at which the ZFC dc magnetization reaches a maximum. The frequency dependence is a direct indication of slow spin dynamics leading us to associate this peak with the SG freezing temperature T_f. This frequency dependence is illustrated more clearly in Fig. 11 which shows a ''closeup'' of this peak in $\chi'(T)$, measured with a temperature spacing of 0.25 K, for the $x=0.09$ sample. We observe the expected SG behavior, with T_f increasing monotonically with increasing frequency f. Moreover, this dependence on frequency is well described by the conventional critical ''slowing down'' of the spin dynamics[53,57] as described by

$$\frac{\tau}{\tau_0}\propto\left(\frac{T_f-T_{\mathrm{SG}}}{T_{\mathrm{SG}}}\right)^{-z\nu}, \tag{4}$$

where $\tau\propto f^{-1}$, T_{SG} is the critical temperature for SG ordering (this is equivalent to the $f\rightarrow 0$ value of T_f), $z\nu$ is a constant exponent, and τ_0 is the characteristic time scale for the spin dynamics. The agreement with Eq. (4) is shown in Fig. 12 for $x=0.09$, where $\log_{10}(f)$ is plotted as a function of $\log_{10}[(T_f-T_{\mathrm{SG}})/T_{\mathrm{SG}}]$. The best fit to the form shown in Eq. (4) is obtained by choosing the value of T_{SG} which minimizes the least-square deviation from a straight-line fit. The values of τ_0 and $z\nu$ are then extracted from the intercept and slope, respectively. For the $x=0.09$ sample this results in the values $T_{\mathrm{SG}}=39.1$ K, $z\nu=9.33$, and $\tau_0=3\times10^{-15}$ s. The T_{SG} value extracted in this manner is clearly reasonable (by a simple extrapolation of T_f to zero frequency), while the other fitting parameters should be compared to canonical SG systems where typical values are $z\nu\approx 10$ and $\tau_0\sim 10^{-13}$ s.[53,57] A similar fitting procedure applied to all samples below $x=0.18$ results in the values shown in Fig. 13. It should be noted that in all cases the chosen value of T_{SG} results in a clear minimum in the least-square deviation from straight-

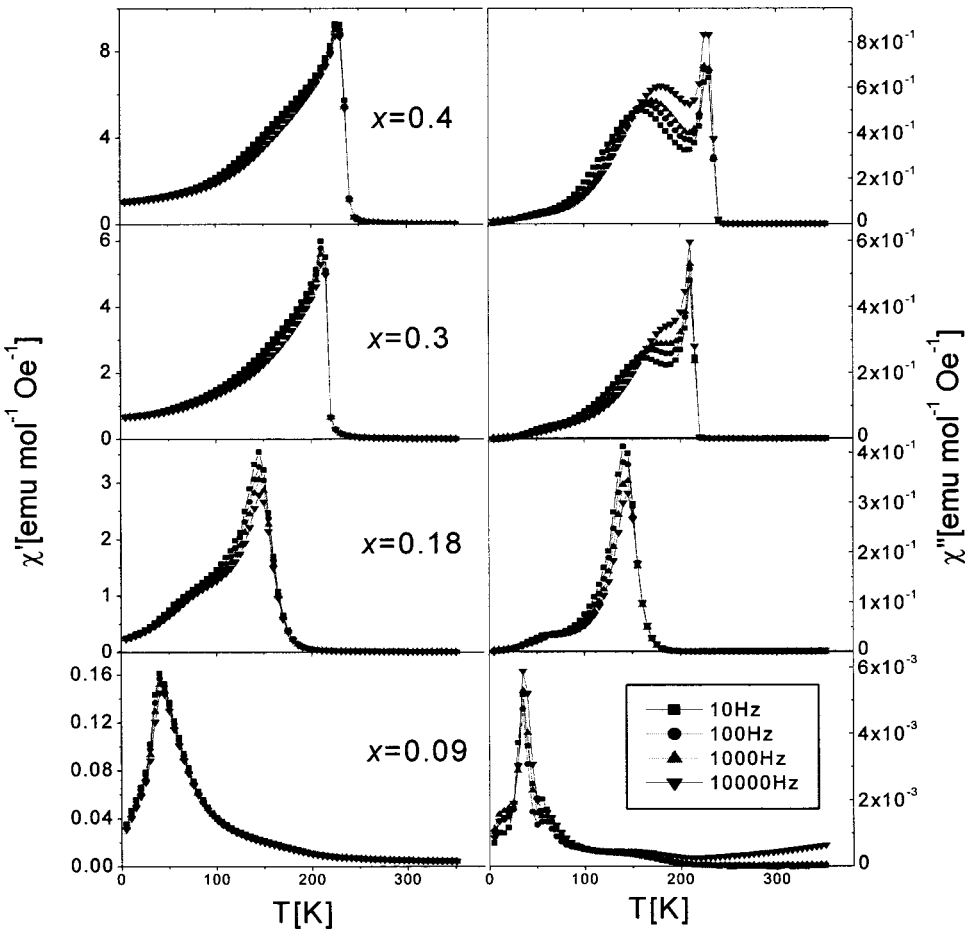

FIG. 10. Temperature dependence of the in-phase (left panel) and out-of-phase (right panel) components of the ZFC ac susceptibility for $x=0.40$ [(a) and (e)], $x=0.30$ [(b) and (f)], $x=0.18$ [(c) and (g)], and $x=0.09$ [(d) and (h)]. The data were taken at 10, 100, 1000, and 10 000 Hz as indicated in the figure.

line behavior in $\log_{10}(f)$ vs $\log_{10}[(T_f-T_{SG})/T_{SG}]$. The data show the expected increase in T_{SG} with x (consistent with the ZFC dc magnetization data) along with a systematic increase in time scale with Sr doping level. These data clearly indicate slower spin dynamics as the doping level increases and cluster sizes grow. As we shall see in the next section of the paper the F phase also displays some glassy characteristics that can be well described by Eq. (1). In this case anomalously large τ_0 values are extracted, consistent with the trend shown in Fig. 13.

It is well known that the out-of-phase component of the ac susceptibility, χ'', provides valuable information on the magnetic energy dissipation or ''energy loss'' over a single cycle of the ac magnetic field. The $\chi''(T)$ behavior is shown in the right-hand panel of Fig. 10, again as a function of frequency of the ac field. $\chi''(T)$ shows a clear evolution in behavior with decreasing x. For the $x=0.40$ and 0.30 samples (in the

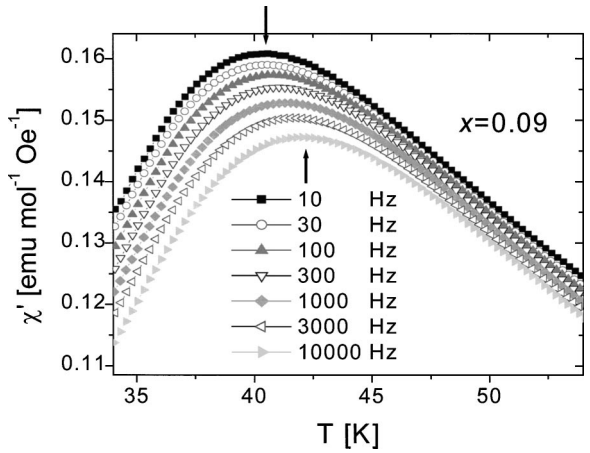

FIG. 11. Closeup of the temperature dependence of the in-phase ac susceptibility for $x=0.09$, at seven frequencies in the range 10–10 000 Hz.

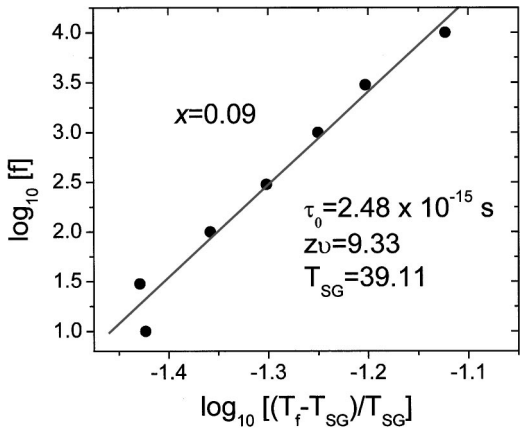

FIG. 12. $\log_{10}(f)$ vs $\log_{10}[(T_f-T_{SG})/T_{SG}]$ for $x=0.09$, demonstrating the agreement with Eq. 1. The solid line is a best fit to the data with the parameters shown in the figure.

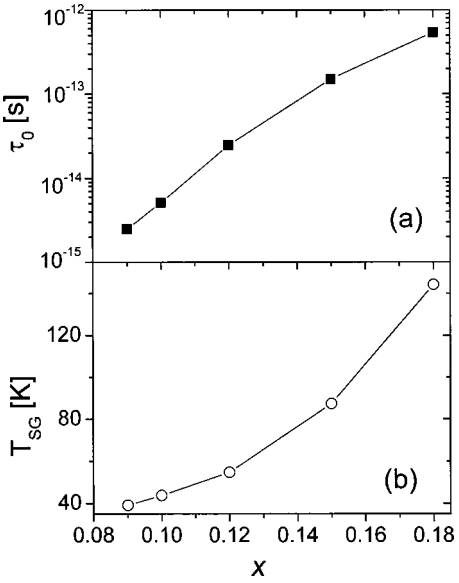

FIG. 13. Doping dependence of the spin-glass freezing temperature (T_{SG}) and relaxation time (τ_0), as extracted from fits of the type shown in Fig. 12.

F phase) we observe a sharp peak in the vicinity of T_C, which is independent of frequency, in addition to a strongly frequency-dependent peak at some $T<T_C$. Close examination of $\chi''(T)$, $\chi'(T)$ (Fig. 7), and the FC $M(T)$ (Fig. 3) reveal that the *peak* in $\chi'(T)$ corresponds to the T_C value extracted from dc $M(T)$, while it is the point at which $\chi''(T)$ approaches zero which corresponds to T_C, rather than the peak in $\chi''(T)$, which actually occurs significantly below T_C. This subtlety has been discussed in detail by Nam and co-workers[20,21] who pointed out that this may indicate that the peaks near T_C in $\chi'(T)$ and $\chi''(T)$ have different origin. In fact they postulate that the peak in $\chi''(T)$ corresponds to the reversibility temperature in dc $M(T)$, where the FC and ZFC magnetizations bifurcate just below T_C.[20,21] We therefore label T_C as the point at which $\chi''(T)$ approaches zero.

The frequency-dependent peak at $T<T_C$ is of greater interest. As shown in Fig. 10 this peak becomes less pronounced and shows reduced frequency dependence as x is lowered towards $x=0.18$. In fact, at the critical value for ferromagnetic order ($x=0.18$), the peak is no longer clearly observed. In this sample the lower temperature side of the main peak in $\chi''(T)$ has now become frequency dependent, suggesting that the two peaks originally observed for $x=0.40$ have actually merged as $x\rightarrow x_c$. At all compositions less than $x=0.18$ (the SG phase), χ'' is considerably reduced in magnitude and simply displays a peak at T_f. The existence of a frequency-dependent peak in $\chi''(T)$ occurring well below T_C is a very clear indication that even in the ''F phase'' these samples do not exhibit conventional long-range ferromagnetic ordering. Rather, it seems natural to ascribe this peak to the freezing of the ferromagnetic clusters which are responsible for the ''Brillouin-like'' FC $M(T)$. Following Nam and co-workers[20,21] we fitted the frequency dependence of this peak to the form in Eq. (4) where the freezing temperature is now the freezing temperature of the ferromagnetic clusters and T_{SG} is replaced by the zero-frequency extrapolation of this cluster freezing temperature, denoted T_{clust}. In agreement with Nam and co-workers we find that the characteristic time scale describing the spin dynamics τ_0 is considerably increased over that found previously for the SG phase (Fig. 13) and the typical values for canonical SG systems.[53] We obtain $\tau_0=4\times10^{-9}$ s for $x=0.30$ and 8×10^{-9} s for $x=0.40$, with $z\nu$ values of 9.38 and 11.66, respectively. Such large characteristic times are no doubt related to the size of the clusters.

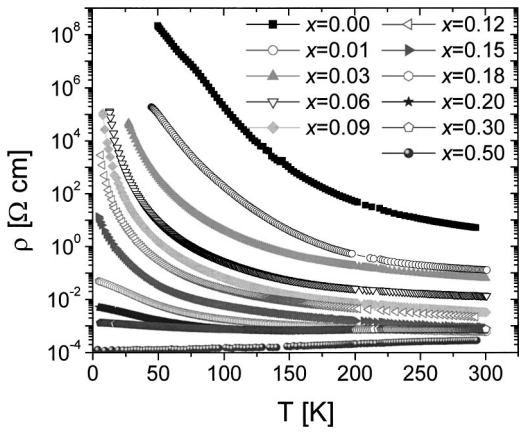

FIG. 14. Temperature dependence of the resistivity of $La_{1-x}Sr_xCoO_3$ in the range $0.00<x<0.50$.

It should be noted that Nam and co-workers[20,21] also measured large aging effects in ''waiting time'' experiments on $x=0.5$ compounds, both below and above the apparent cluster freezing temperature. These data represent further evidence of the glassy nature of the ferromagnetically ordered state at $x>0.18$.

In summary, the ac susceptibility of $La_{1-x}Sr_xCoO_3$ evolves in a systematic way as x is lowered from the F regime into the SG dominated phase. In the F dominated regime $\chi'(T)$ shows a frequency-independent peak at T_C which occurs at a lower temperature as x is lowered. When the SG phase is entered this peak becomes frequency dependent and marks the SG freezing temperature. On the other hand $\chi''(T)$ increases from zero at T_C to form a frequency-independent peak in the F phase. This is followed by a second peak at $T\ll T_C$, which shows a strong frequency dependence and has been interpreted as the point at which the ferromagnetic clusters freeze. Unsurprisingly the dynamics of this process become slower as x is increased and the ferromagnetic clusters become more dominant.

C. Magnetotransport

As expected, doping divalent Sr onto the trivalent La sites in the semiconductor $LaCoO_3$ results in hole doping and the eventual onset of metallic behavior. The evolution of the temperature dependence of the resistivity with Sr doping is displayed in Fig. 14. Note again that more compositions were measured but only 11 are shown for the purposes of clarity. The $x=0$ end point, $LaCoO_3$, shows semiconducting behavior as $T\rightarrow0$, along with a small anomaly in the vicinity

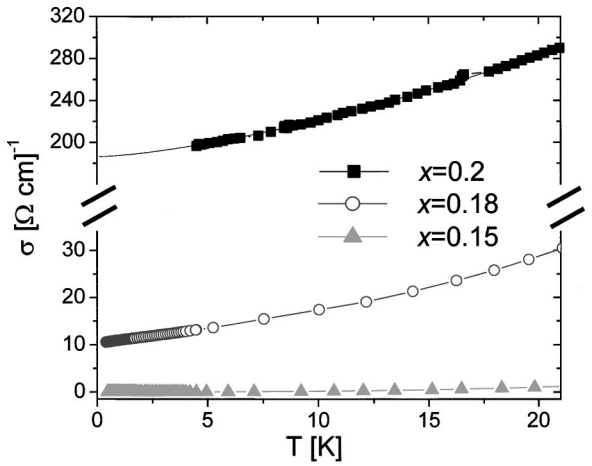

FIG. 15. Temperature dependence ($0.40 < T < 20$ K) of the conductivity for $x = 0.15$, 0.18, and 0.20. Note the ''split'' conductivity scale.

of the spin-state transition at 100 K, as detailed elsewhere.[16] Sr doping rapidly decreases $\rho(T=0)$ and eventually leads to a metallic like temperature dependence ($d\rho/dT > 0$) for $x > 0.20$. Concerning the exact position of the MIT it is important to note the qualitative differences between $\rho(T)$ for $x = 0.15$ and $x = 0.18$. In the former case $\rho(T)$ appears to be diverging at $T = 0$, indicating that the system is on the insulating side of the MIT. On the other hand the $x = 0.18$ sample appears to show a weakening in $\rho(T)$ as $T \to 0$, and would appear to have a finite value for the zero-temperature extrapolation of the conductivity, i.e., metallic behavior. (Here we are using the rigorous definition of a metal—a material with a finite (nonzero) conductivity at the absolute zero of temperature.) This is shown more clearly in Fig. 15, which displays the temperature dependence of the low-temperature conductivity σ for $x = 0.15$, 0.18, and 0.20. Measurement of the $\sigma(T)$ curves for $x = 0.15$ and $x = 0.18$ was extended to 0.4 K in order to make a more meaningful assessment of the zero-temperature conductivity. Given the nonzero value for the zero-temperature extrapolation of the conductivity for $x = 0.18$, we conclude that the MIT lies in the range $0.15 < x_C < 0.18$. The dependence of the 5 K conductivity on x is shown in Fig. 16 (both on linear and $\log_{10}$ scales), where we see that the onset of metallic behavior is quite sharp and is followed by an immediate saturation of the conductivity. The data clearly show that the critical Sr doping level for the onset of ferromagnetic order ($x_c \approx 0.18$) is identical to the MIT critical point. This is in contrast to the manganite system $La_{1-x}Sr_xMnO_3$ where ferromagnetism is achieved at a much lower Sr doping than the onset of metallicity.[2] In fact the phase that is classified as ''ferromagnetic insulator'' ($x > 0.09$) occurs before the ''ferromagnetic metal'' phase is entered ($x > 0.16$).[2] This is also true of numerous other phase diagrams in the manganite series.[2] The simultaneous onset of ferromagnetism and metallicity in our cobaltite system leads us to propose that the two are related. Specifically we suggest that the critical Sr doping value x_c is the point at which the ferromagnetically ordered (hole-rich) clusters begin to coalesce and percolation occurs. This leads to metallic behavior in $\rho(T)$ and ferromagnetlike behavior in $M_{FC}(T)$. In this simple model we would expect that the behavior of σ ($T \to 0$) as a function of x would be more consistent with a percolation transition than a conventional Mott-Anderson transition. At conventional $T = 0$ MIT's the conductivity is expected to follow the form

$$\sigma(T \to 0) = \sigma_0 \left(\frac{x}{x_C} - 1 \right)^{\mu} \tag{5}$$

from the scaling theory of electron localization.[58] In this equation σ_0 is a constant prefactor while μ is the conductivity critical exponent. The value of the exponent has been a matter of experimental and theoretical debate since the introduction of the scaling theory, but is found to lie in the range $0.5 < \mu < 1.0$ in the vast majority of cases.[59] The situation for a percolation transition is very different; again a number of values have been proposed for μ but they are in the region of $\mu \approx 1.6$–2.0.[60] For the specific situation of a mixed valence manganite system Xiong *et al.*[61] calculated the critical exponent for a percolation transition, finding, in agreement with earlier experiments,[62] that the exponent is significantly larger than 1 and is strongly magnetic-field dependent. Although the data in Fig. 16(a) do show a rounded transition followed by a rapid increase in σ with increasing x (i.e., they would appear consistent with $\mu \gg 1.0$) the elevated temperature (5 K) produces significant thermal smearing of the transition region.[63] Future work will include extending these measurements to below 1 K to investigate this issue in detail. It is also clear that this would require investigation of a larger number of samples in the critical region.

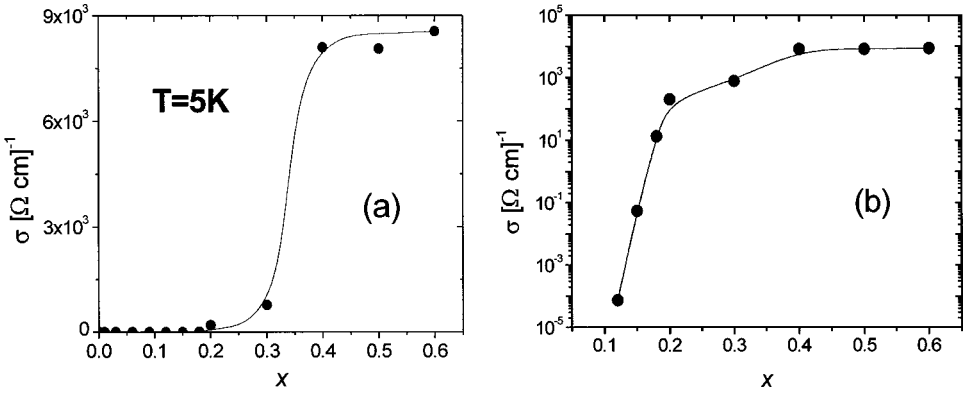

FIG. 16. Sr doping dependence of the 5 K conductivity (a) on a linear scale and (b) on a $\log_{10}$ scale. The solid line is a guide to the eye.

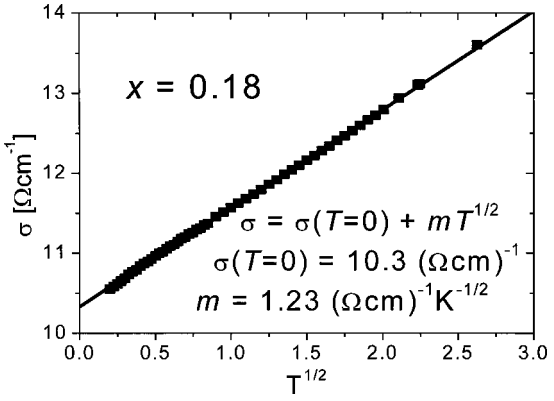

FIG. 17. Temperature dependence of the conductivity for $x=0.18$ plotted on a $T^{1/2}$ scale.

The most striking feature of the data shown in Fig. 16 is not the details of the onset of metallic behavior (which were just discussed), but the saturation of the conductivity immediately after the metallic phase is entered. This behavior is reminiscent of the simplest possible scenario for a percolation transition where one of the phases is metallic with a finite conductivity and the other is insulating with zero conductivity at $T=0$. After the percolation limit is exceeded and metallic paths become present the conductivity saturates at the conductivity of the metallic phase. An alternative explanation is that the conductivity is limited by grain boundary scattering in these polycrystalline specimens. We reject this hypothesis on the grounds that the conductivity saturates at unreasonably low values for a grain size, which is known to be in the μm range. Assuming a simple free-electron model and reasonable values for the free-carrier density we calculate that the conductivity at which we observe saturation corresponds to a mean free path of the order of 10 nm, i.e., at least 100 times lower than the grain size. In order to obtain a mean free path comparable to the grain size for these conductivity values we would have to accept a carrier density as low as 10^{18} cm^{-3}. Although free-electron models are unlikely to account exactly for the metallic conductivity in systems such as these, it seems that the conductivity saturation shown in Fig. 16 is not due to grain-boundary scattering. We therefore interpret the data in terms of the simple percolation model.

The temperature dependence of the conductivity near the MIT is worthy of further comment. As expected from the effects of electron-electron interaction in the presence of disorder, Sr doping levels just on the metallic side of the transition exhibit a $T^{1/2}$ dependence in the conductivity.[59] As shown in Fig. 17, for $x=0.18$, the conductivity obeys $\sigma(T)=\sigma(T=0)+mT^{1/2}$,[59] with $\sigma(T=0)=10.3\ (\Omega\ \mathrm{cm})^{-1}$ and $m=1.23\ (\Omega\ \mathrm{cm})^{-1}\,\mathrm{K}^{-1/2}$, below about 10 K. Such m values are in good agreement with previous work on disordered systems near the MIT.[59,48] This analysis cannot be applied to higher x samples because (i) it only applies in the weakly localized regime close to the MIT and (ii) samples with $x>0.20$ were not measured below 5 K. On the insulating side of the MIT the data of Fig. 14 for $x<0.18$ where found to fit the Mott variable range hopping law, $\sigma=A\exp[-(T_0/T)^{1/4}]$, where A and T_0 are constants. T_0 shows a dramatic reduction with increasing x (as the MIT is approached), falling from 3.3×10^7 K for $x=0.03$ to 2×10^4 K at $x=0.15$. This can be understood based on the fact that T_o scales as $1/\xi^3$, where ξ, the localization length, diverges at the MIT in accordance with the scaling theory.[58,59]

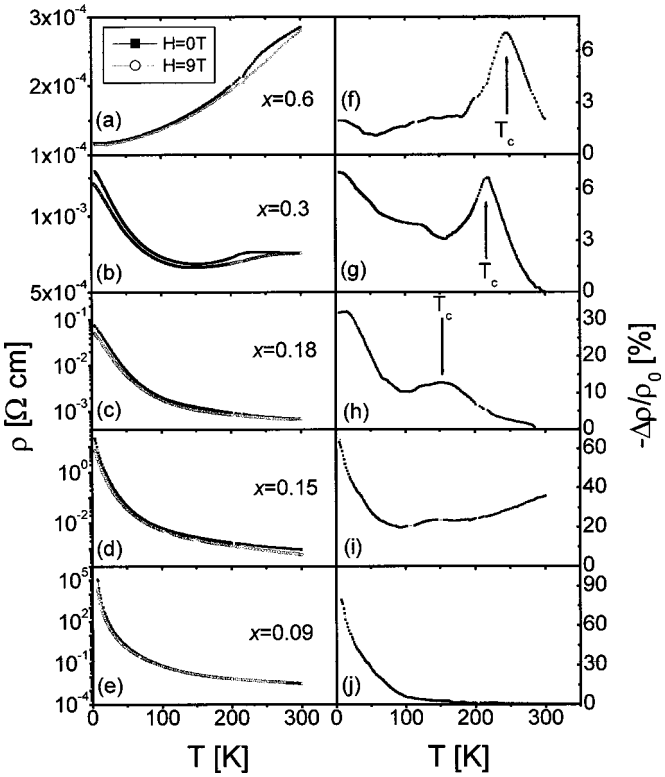

FIG. 18. Temperature dependence of the resistivity (left panel) and magnetoresistance (right panel) for $x=0.60$ [(a) and (f)], $x=0.30$ [(b) and (g)], $x=0.18$ [(c) and (h)], $x=0.15$ [(d) and (i)], and $x=0.09$ [(e) and (j)]. The resistivity data were taken in zero field (closed symbols) and 90 kOe (open symbols). All of the MR values are for 90 kOe. The arrows indicate the value of T_C for the ferromagnetic samples.

The behavior of the magnetoresistance (MR) ratio $[\Delta\rho/\rho_0=\rho(H)-\rho(H=0)/\rho(H=0)]$ and a closer examination of $\rho(T,H)$ are shown in Fig. 18. Samples with $x=0.60$, 0.30, 0.18, 0.15, and 0.09 are shown, and the MR data were taken in a magnetic field of 90 kOe. The $x=0.60$ and 0.30 samples are representative of the F phase, showing metallic behavior in $\rho(T)$ and a negative MR which peaks in the vicinity of T_C. At the most conductive compositions (around $x=0.4$–0.6) $d\rho/dT>0$ in the whole T range, and MR values up to 10% can be achieved. We consider this MR to be a CMR-type behavior similar to that observed in $La_{0.67}Sr_{0.33}MnO_3$,[2,3,10,11,63] due to the fact that it is negative, peaks just below T_C and has the expected field dependence, as shown in Fig. 19. Here it is clearly seen that the $\rho(H)$ behavior is "rounded" above T_C and "sharp" below T_C. This is due to the fact that the MR scales with the sample magnetization,[2,3,63] meaning that the resistivity decreases quickly with applied field for $T<T_C$, where M increases rapidly with H. There are a number of noteworthy points about the behavior of the CMR, which should be addressed

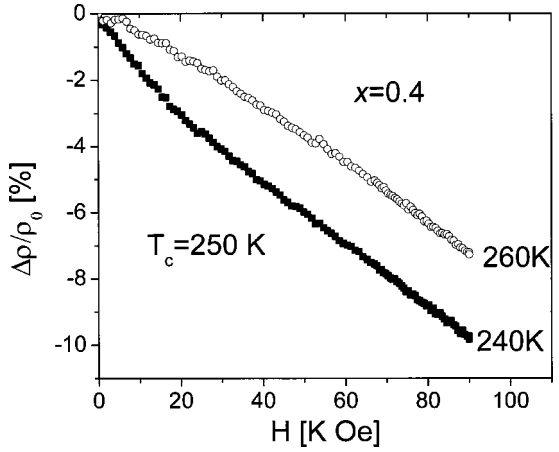

FIG. 19. Magnetic field dependence of the magnetoresistance ratio for $x=0.40$. The data were taken just above (260 K) and just below (240 K) T_C (250 K).

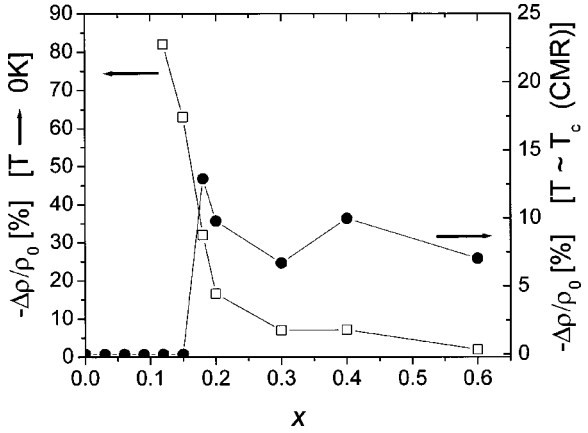

FIG. 20. The doping dependence of the two magnetoresistance contributions. The open symbols denote the low-temperature (5 K) MR, while the solid symbols represent the CMR-type behavior, which occurs in the vicinity of T_C.

before we continue to a description of the magnetotranport behavior as x is decreased and the MIT occurs. First, the low-temperature tail in MR(T) for the most conductive samples [e.g., $x=0.6$ in Fig. 18(b)] is rather small. This tail is typically observed in polycrystalline manganite thin films and bulk samples but is not observed in single crystals.[3,64–66] It is attributed to intergranular tunneling across grain boundaries, an effect analogous to the tunneling magnetoresistance (TMR) observed in planar F/insulator/F tunnel junctions.[67] It is therefore accompanied by hysteresis in $\rho(H)$ and increases strongly with decreasing temperature. Our samples display neither of these effects; we observe no hysteresis in the MR and, at least for the most conductive part of the phase space, the MR does not increase sharply with decreasing T. We therefore doubt that the low-T MR is due to the intergranular tunneling mechanism. It is also worth noting that we observe none of the complex, history dependent, resistivity nonclosure effects observed in a previous study of the MR of $La_{1-x}Sr_xCoO_3$ polycrystals by Mahendiran *et al.*[68] Mahendiran *et al.* also report an unexpected crossover to positive MR at high T for the most metallic samples. We do not observe such behavior.

As x is lowered and the MIT is approached this low T tail in MR(T) becomes more pronounced, as does an upturn in $\rho(T)$ at low temperatures, likely due to weak localization. [Given that we have conclusively proven that samples with $x>0.18$ have finite zero-temperature conductivity and are therefore metals we interpret the low-T upturn in $\rho(T)$ simply as due to weak localization, rather than a re-entrant insulator-metal transition as suggested by Senaris-Rodriguez *et al.*[56]] As x is reduced to 0.18 and below, the CMR peak in the vicinity of T_C decreases in magnitude and eventually disappears, the low-T MR increases and $\rho(T)$ crosses over to a semiconductorlike temperature dependence. $x=0.18$ is the lowest x which shows a peak in MR(T), further evidence that the critical composition lies in the range $0.15<x_c<0.18$. The dependence of the MR on x is more clearly shown in Fig. 20, which plots the peak MR value (due to CMR effects) and the maximum low-T MR (measured at 5 K) as a function of x. The CMR peak vanishes sharply at x_c, while the low-T MR monotonically increases with decreasing x, as the insulating phase is entered. The behavior just below the MIT at $x=0.15$ is particularly interesting [Fig. 17(h)], as the MR persists even up to room temperature where it attains a value of approximately 35%. The origin of this MR is not completely clear although it is likely due to spin-dependent effects in the hopping regime. These effects are due to the spin-dependent part of the random potential distribution, which is suppressed in large magnetic fields as the spins are aligned. The behavior in the magnetic semiconductor $Gd_{3-x}v_xS_4$ as investigated by von Molnar *et al.*[47] is the classic example. Very similar behavior has previously been observed by us in $LaCoO_3$ above the spin-state transition temperature,[16] where the Co^{3+} ions are paramagnetic. It is important to note that the work on classic magnetic semiconductors such as $Gd_{3-x}v_xS_4$ (Ref. 47) and $Cd_{1-x}Mn_xTe$:In (Ref. 48) shows that the behavior of the MR in the insulating phase can be understood in terms of the formation of magnetic polarons. The polarons are aligned by the magnetic field leading to a suppression of the spin-dependent part of the disorder potential and increased probability for a hop.[47] In our cobaltite system the situation is similar. The Co^{3+} and Co^{4+} spins which make up the magnetic polarons (or ferromagnetic clusters) are aligned by the magnetic field leading to an increased hopping probability and a negative MR. This simple, albeit very qualitative, model also offers a possible explanation for the enhancement of the MR near the MIT, leading to MR persisting to room temperature for $x=0.15$. In the situation where the composition is very close to the percolation threshold it is clear that the application of a magnetic field, which changes the spin alignment of the clusters is likely to induce large changes in the conductivity. This is consistent with the concepts developed by Xiong *et al.*[61] where the critical exponent for the percolation driven MIT is a strong function of magnetic field.

It is important to note that the SG freezing appears to have no effect on ρ or the MR. There are no anomalies at T_f at any of the compositions studied. The effect of SG freezing

on the transport properties of magnetic semiconductors is a relatively open issue and there are few cases where T_f influences the conduction mechanism. Rare examples include a-Mn_xSi_{1-x} (Ref. 69) and $Cd_{1-x}Mn_xTe$:In,[70] where the SG freezing leads to a corresponding freezing of the magnetic polaron binding energy, which in turn leads to the recovery of a simple activated form for $\rho(T)$ in the hopping regime.

As a final note on the magnetotransport properties of this system and their relation to the ferromagnetic clusters and percolation, we would like to point out that a similar model is invoked to explain the observation of a giant anomalous Hall effect in single-crystal $La_{1-x}Ca_xCoO_3$.[71] The original discovery of the largest anomalous Hall effect of any known metal was made in $La_{1-x}Ca_xCoO_3$ thin films by Samoilov *et al.*[72] who interpreted their data in terms of enhanced spin-orbit scattering at the interfaces between low-spin and high-spin regions, in the vicinity of the percolation threshold. Baily *et al.*[71] prefer to interpret the giant anomalous Hall effect as being due to an inhomogeneous current density due to the existence of ferromagnetic clusters. This second scenario is entirely consistent with the cluster model used in this paper to understand the magnetotransport properties of $La_{1-x}Sr_xCoO_3$.

To summarize our magnetotransport measurements we observe a MIT at x_c which is consistent with a percolation transition. The ferromagnetic clusters begin to coalesce at this point leading to the simultaneous onset of ferromagnetism. CMR-type behavior is observed on the metallic side of the MIT, while a low-T component to the MR increases in magnitude as the insulating phase is entered. This MR contribution is attributed to the increase in the probability of hopping processes as the external field aligns the Co spins, leading to negative MR.

IV. SUMMARY AND CONCLUSIONS

We have presented a detailed set of magnetometry, ac susceptibility and magnetotransport measurements on polycrystals of $La_{1-x}Sr_xCoO_3$ at a total of 14 compositions from $x=0$ ($LaCoO_3$) to $x=0.7$. The magnetic phase diagram has been constructed and the characteristics of each phase established. In the ferromagnetic phase measurements of the average spin state of the Co ions, from both Brillouin function fits to the temperature dependence of the magnetization and Curie-Weiss behavior at high temperatures, indicated a composition dependence that is consistent with both ions adopting the intermediate-spin state. At $x \geqslant 0.18$ we observe indications of ferromagnetic ordering (large magnetization, Brillouin-like temperature dependence of the field cooled magnetization and the existence of a Curie temperature) as well as simultaneous indications of glassy behavior (frequency-dependent peaks in the out-of-phase component of the ac susceptibility and an unusual temperature dependence of the zero-field-cooled magnetization). On the other hand, for $x<0.18$ we observe clear indications of spin-glass freezing (a frequency-dependent peak in the in-phase component of the ac susceptibility which can be described by critical slowing down of spin dynamics) as well as indications of strong ferromagnetic correlations (large field-cooled magnetization). In terms of magnetotransport properties we have determined that the metal to insulator transition is coincident with the onset of ferromagnetic ordering. On the metallic side we observe colossal magnetoresistance-type effects which exhibit a peak in the vicinity of the Curie temperature. In contrast, the magnetoresistance on the semiconducting side monotonically increases with decreasing temperature and shows an enhancement near the transition. We have consistently interpreted all of these phenomena in terms of the short-range-ordered ferromagnetic cluster model, which seems to be a very reasonable qualitative description of the phenomenology. This system clearly shows a propensity for intrinsic phase separation that is even stronger than that seen in manganites such as $La_{1-x}Sr_xMnO_3$. We suggest that the evidence for magnetic phase separation in doped cobaltites is abundant, and that these compounds are model systems in which to study intrinsic phase separation. Future experiments which would greatly benefit the understanding of the fundamentals of phase separation include transmission electron microscopy, neutron scattering, scanning tunneling microcopy, scanning tunneling spectroscopy, and Co nuclear magnetic resonance. In addition it is clear that quantitative models of the phase separation are needed along with predictions concerning the size, magnetization, carrier density, and spin dynamics of the ferromagnetically correlated clusters.

ACKNOWLEDGMENTS

We would like to thank I. Terry, W. Moulton, D. Dahlberg, P. Crowell, and S. Giblin for valuable discussions. We are grateful to the UMN Institute for Rock Magnetism for the use of magnetometry facilities. The acquisition of a measurements system which was used extensively in this investigation was supported by NSF Grant No. DMR-0113917.

[1] G. Burns, *High Temperature Superconductivity—An Introduction* (Academic, Boston, 1992); R. Wesche, *High Temperature Superconductors: Materials Properties and Applications* (Kluwer Academic, Boston, 1998).

[2] Y. Tokura and Y. Tomioka, J. Magn. Magn. Mater. **200**, 1 (1999).

[3] J. M. D. Coey, M. Viret, and S. von Molnár, Adv. Phys. **48**, 167 (1999).

[4] R. Ramesh, B. Dutta, T. S. Ravi, J. Lee, T. Sands, and V. G. Keramidas, Appl. Phys. Lett. **64**, 1588 (1994).

[5] M. K. Lee, T. K. Nath, C. B. Eom, M. C. Smoak, and F. Tsui, Appl. Phys. Lett. **77**, 3547 (2000).

[6] A. Moreira dos Santos, A. K. Cheetham, T. Atou, Y. Syono, Y. Yamaguchi, K. Ohoyama, H. Chiba, and C. N. R. Rao, Phys. Rev. B **66**, 064425 (2002).

[7] N. A. Hill and A. Filippetti, J. Magn. Magn. Mater. **242–245**, 976 (2002).
[8] W. C. Koehler and E. O. Wollan, J. Phys. Chem. Solids **2**, 100 (1957).
[9] R. R. Heikes, R. C. Miller, and R. Mazelsky, Physica (Amsterdam) **30**, 1600 (1964).
[10] R. von Helmolt, J. Wecker, B. Holzapfel, L. Schultz, and K. Samwer, Phys. Rev. Lett. **71**, 2331 (1993).
[11] S. Jin, M. McCormack, T. H. Tiefel, and R. Ramesh, J. Appl. Phys. **76**, 6929 (1994); H. L. Ju, C. Kwon, Q. Li, R. L. Greene, and T. Venkatesan, Appl. Phys. Lett. **65**, 2108 (1994); Y. Tokura, A. Urushibara, Y. Moritomo, T. Arima, A. Asamitsu, G. Kido, and N. Furukawa, J. Phys. Soc. Jpn. **63**, 3931 (1994).
[12] For a short review, see M. Imada, A. Fujimori, and Y. Tokura, Rev. Mod. Phys. **70**, 1039 (1998).
[13] K. Asai, P. Gehring, H. Chou, and G. Shirane, Phys. Rev. B **40**, 10 982 (1989).
[14] S. Yamaguchi, Y. Okimoto, and Y. Tokura, Phys. Rev. B **55**, R8666 (1997).
[15] C. Zobel, M. Kriener, D. Bruns, J. Baier, M. Gruninger, T. Lorenz, P. Reutler, and A. Revcolevschi, Phys. Rev. B **66**, 020402 (2002).
[16] S. R. English, J. Wu, and C. Leighton, Phys. Rev. B **65**, 220407(R) (2002).
[17] F. Faith, E. Suard, and V. Caignert, Phys. Rev. B **65**, 060401 (2001).
[18] P. Ravindran, H. Fjellvag, A. Kjekshus, P. Blaha, K. Schwarz, and J. Luitz, J. Appl. Phys. **91**, 291 (2002).
[19] M. A. Korotin, S. Yu. Ezhov, I. V. Solovyey, V. I. Anisimov, D. I. Khomskii, and G. A. Sawatzky, Phys. Rev. B **54**, 5309 (1996).
[20] D. N. H. Nam, K. Jonason, P. Nordblad, N. V. Khiem, and N. X. Phuc, Phys. Rev. B **59**, 4189 (1999); D. N. H. Nam, R. Mathieu, P. Nordblad, N. V. Khiem, and N. X. Phuc, *ibid.* **62**, 8989 (2000).
[21] N. X. Phuc, N. V. Khiem, and D. N. H. Nam, J. Magn. Magn. Mater. **242–245**, 754 (2002).
[22] S. Mukherjee, R. Ranganathan, P. S. Anilkumar, and P. A. Joy, Phys. Rev. B **54**, 9267 (1996).
[23] K. Asai, O. Yokokura, N. Nishimori, H. Chou, J. M. Tranquada, G. Shirane, S. Higuchi, Y. Okajima, and K. Kohn, Phys. Rev. B **50**, 3025 (1994).
[24] M. Itoh, I. Natori, S. Kubota, and K. Motoya, J. Magn. Magn. Mater. **140–144**, 1811 (1995).
[25] S. Tsubouchi, T. Kyomen, M. Itoh, P. Ganguly, M. Oguni, Y. Shimojo, Y. Mori, and Y. Ishii, Phys. Rev. B **66**, 052418 (2002).
[26] S. Roy, M. Khan, Y. Q. Guo, J. Craig, and N. Ali, Phys. Rev. B **65**, 064437 (2002).
[27] C. Frontera, J. L. Garcia-Munoz, A. Llibet, M. A. G. Aranda, J. Rodriguez-Carvajal, M. Respaud, J. M. Broto, B. Raquet, H. Rakato, and M. Goiran, J. Magn. Magn. Mater. **242–245**, 751 (2002).
[28] R. Mathieu, P. Nordblad, D. N. H. Nam, N. X. Phuc, and N. V. Khiem, Phys. Rev. B **63**, 174405 (2001).
[29] D. Sedmidubsky, J. Hejtmanek, M. Marysko, Z. Jirak, V. Hardy, and C. Martin, J. Appl. Phys. **91**, 8260 (2002).
[30] R. S. Freitas, L. Ghivelder, F. Damay, F. Dias, and L. F. Cohen, Phys. Rev. B **64**, 144404 (2001).
[31] A. K. Pradhan, Y. Feng, S. Shibata, K. Nakao, and N. Koshizuka, Europhys. Lett. **56**, 105 (2001).
[32] Y. Breard, C. Michel, A. Maignan, and B. Raveau, Solid State Commun. **118**, 517 (2001).
[33] A. Maignau, C. Martin, M. Hervieu, and B. Raveau, Eur. Phys. J. B **13**, 41 (2000).
[34] Z. H. Wang, X. Chen, B. G. Shen, Y. D. Zhang, J. W. Cai, R. W. Li, J. G. Zhao, and W. S. Zhan, Phys. Rev. B **60**, 14 541 (1999).
[35] S. H. Chun, Y. Lyanda-Geller, M. B. Salamon, R. Suryanarayanan, G. Dhalene, and A. Revcolevschi, J. Appl. Phys. **90**, 6307 (2001).
[36] J. Dho, W. S. Kim, and N. H. Hur, Phys. Rev. Lett. **89**, 027202 (2002).
[37] J. W. Lynn, R. W. Erwin, J. A. Borchers, Q. Huang, A. Santoro, J.-L. Peng, and Z. Y. Li, Phys. Rev. Lett. **76**, 4046 (1996); J. A. Fernandez-Baca, P. Dai, H. Y. Hwang, C. Kloc, and S.-W. Cheong, *ibid.* **80**, 4012 (1998).
[38] M. Fath, S. Freisem, A. A. Menovsky, Y. Tomioka, J. Aarts, and J. A. Mydosh, Science (Washington, DC, U.S.) **285**, 1540 (1999).
[39] B. Raquet, A. Anane, S. Wirth, P. Xiong, and S. von Molnar, Phys. Rev. Lett. **84**, 4485 (2000).
[40] B. Raquet, in *Spin Electronics*, edited by M. Ziese and M. J. Thornton (Springer, New York, 2001), p. 232.
[41] P. Levy, F. Parisi, L. Granja, E. Indelicato, and G. Polla, Phys. Rev. Lett. **89**, 137001 (2002).
[42] E. Dagotto, T. Hotta, and A. Mareo, Phys. Rep. **344**, 1 (2001).
[43] J. Burgy, M. Mayr, V. Martin-Mayor, A. Moreo, and E. Dagotto, Phys. Rev. Lett. **87**, 277202 (2001).
[44] T. Shibata, B. Bunker, J. F. Mitchell, and P. Schiffer, Phys. Rev. Lett. **88**, 207205 (2002).
[45] For a short review, see Ref. 3, p. 178.
[46] F. Hellman, M. Q. Tran, A. E. Gebala, E. M. Wilcox, and R. C. Dynes, Phys. Rev. Lett. **77**, 4652 (1996); B. L. Zink, E. Janod, K. Allen, and F. Hellman, *ibid.* **83**, 2266 (1999).
[47] For a short review, see Ref. 3, p. 183.
[48] D. E. Read, C. Leighton, I. Terry, and P. Becla, Ann. Phys. (Leipzig) **8**, 217 (1999); C. Leighton, I. Terry, and P. Becla, Phys. Rev. B **58**, 9773 (1998); I. Terry, T. Penney, S. von Molnar, and P. Becla, J. Cryst. Growth **159**, 1070 (1996).
[49] T. Kasuya, A. Yanase, and T. Takeda, Solid State Commun. **8**, 1543 (1970); T. Kasuya, A. Yanase, and T. Takeda, Solid State Commun. **8**, 1551 (1970).
[50] J. Wu and C. Leighton (unpublished).
[51] A Curie-Weiss fit to the temperature dependence of the susceptibility above the spin-state transition near 100 K results in an antiferromagnetic θ value of approximately -200 K (see Ref. 16).
[52] J. de Almeida and D. Thouless, J. Phys. A **11**, 983 (1978).
[53] J. A. Mydosh, *Spin-Glasses: An Experimental Introduction* (Taylor and Francis, London, 1993).
[54] S. Yamaguchi, Y. Okimoto, H. Taniguchi, and Y. Tokura, Phys. Rev. B **53**, R2926 (1996).
[55] R. Caciuffo, D. Rinaldi, G. Barucca, J. Mira, J. Rivas, M. A. Senaris-Rodriguez, P. G. Radaelli, D. Forani, and J. B. Goodenough, Phys. Rev. B **59**, 1068 (1999); J. Mira, J. Rivas, G. Baio, G. Barucca, R. Caciuffo, D. Rinaldi, D. Fiorani, and M. A. Senaris-Rodriguez, J. Appl. Phys. **89**, 5606 (2001).
[56] M. A. Señarís-Rodríguez and J. B. Goodenough, J. Solid State Chem. **118**, 323 (1995).
[57] K. Gunnarson, P. Svedlindh, P. Nordblad, L. Lundgren, H. Aruga, and A. Ito, Phys. Rev. Lett. **61**, 754 (1988).

[58] E. Abrahams, P. W. Anderson, D. C. Licciardello, and T. V. Ramakrishnan, Phys. Rev. Lett. **42**, 673 (1979).
[59] W. Sasaki, in *Anderson Localization*, edited by T. Ando and H. Fukuyama (Springer-Verlag, Berlin, 1988), p. 10; P. A. Lee and T. V. Ramakrishnan, Rev. Mod. Phys. **57**, 287 (1985).
[60] B. I. Shklovskii and A. L. Efros, *Electronic Properties of Doped Semiconductors* (Springer-Verlag, Berlin, 1984), p. 105.
[61] Y. Xiong, S.-Q. Shen, and X. C. Xie, Phys. Rev. B **63**, 140418(R) (2001).
[62] M. Uehara, S. Mori, C. H. Chen, and S. W. Cheong, Nature (London) **399**, 560 (1999).
[63] R. M. Westervelt, M. I. Burns, P. F. Hopkins, A. J. Rimberg, and G. A. Thomas, in *Anderson Localization*, edited by T. Ando and H. Fukuyama (Springer-Verlag, Berlin, 1988), p. 33.
[64] M. Viret, in *Spin Electronics*, edited by M. Ziese and M. J. Thornton (Springer, New York, 2001), p. 117.
[65] S. Lee, H. Y. Wang, B. I. Shraiman, W. D. Ratcliff II, and S.-W. Cheong, Phys. Rev. Lett. **82**, 4508 (1999).
[66] A. Maignan, C. Martin, M. Hervieu, and B. Raveau, J. Magn. Magn. Mater. **211**, 173 (2000).
[67] J. S. Moodera and G. Mathon, J. Magn. Magn. Mater. **200**, 248 (1999).
[68] R. Mahendiran and A. K. Raychaudari, Phys. Rev. B **54**, 16 044 (1996).
[69] A. I. Yakimov, A. V. Dvurechenskii, and C. J. Adkins, Phys. Status Solidi B **205**, 299 (1998).
[70] I. Terry, T. Penney, S. von Molnar, and P. Becla, Phys. Rev. Lett. **69**, 1800 (1992).
[71] S. A. Baily, M. B. Salamon, Y. Kobayashi, and K. Asai, Appl. Phys. Lett. **80**, 3138 (2002).
[72] A. V. Samoilov, G. Beach, C. C. Fu, N.-C. Yeh, and R. P. Vasquez, Phys. Rev. B **57**, R14 032 (1998); N.-C. Yeh, C. C. Fu, X. Xie, R. P. Vasquez, and A. V. Samoilov, Physica B **284–288**, 1446 (2000).